ISSN 1064-2269, Journal of Communications Technology and Electronics, 2022, Vol. 67, No. 7, pp. 854–875. © Pleiades Publishing, Inc., 2022.

THEORY AND METHODS OF SIGNAL PROCESSING

Statistical Analysis of 5G/6G Millimeter Wave Channels for Different Scenarios

A. Bedda-Zekri[a] and R. Ajgou[b, *]

[a] *LEVRES Laboratory, Department of Electrical Engineering, University of El Oued, 39000 El-Oued Algeria*

[b] *LGEERE Laboratory, Department of Electrical Engineering, University of El Oued, 39000 El-Oued Algeria*

**e-mail: riadh-ajgou@univ-eloued.dz*

Received October 3, 2020; revised January 21, 2022; accepted February 2, 2022

Abstract—The fifth-generation (5G) wireless communication deployment has already begun. However, some technical problems that need to be updated and further technological improvements are needed. In 5G NR (New Radio), the wide ranges of radio spectrum, from 30 to 300 GHz and 0.1 to 10 THz, referred to as millimeter waves (mm Waves) and sub-terahertz respectively, remain unemployed. These ranges can offer a great opportunity to cope with the huge expansion in data and connectivity in today's mobile society. For this concern, this paper provides an in-depth statistical study of millimeter wave propagation candidates for 5G/6G systems (28, 38, 60, 73, 100, and 120 GHz) based on different scenarios for outdoor Urban Microcell (UMi) channels with various scenarios especially the geometrical parameters (Co-Pol/X-Pol, SISO/SIMO/MIMO), and also the environmental conditions (LOS/NLOS, rain rate, temperature and humidity for an urban Microcell). The results indicated that the 38 and 73 GHz channels are quite tolerant to the impact of deteriorating environmental conditions and geometrical parameter variations, while the 60, 100 and 120 GHz channels are more affected. In terms of path loss (PL) and path loss exponent (PLE), the omni-directional power delay profile (OPDP) showed improved performance over the directional power delay profile (DPDP) for all channels.

Keywords: path loss, mmWaves, sub-terahertz, LOS/NLOS, OPDP, DPDP

DOI: 10.1134/S1064226922070063

INTRODUCTION

Without waiting for the launch of 5G mobile networks around the world, the competition for 6G has already started. Researchers are promised a 6G technology that would further amplify the benefits of 5G for more data rate, more connected devices, and on a more secure network with less intensive energy. In terms of data rates, if 5G brings wireless user terminals into the gigabit era, 6G will propel us a thousand times faster, at speeds reaching 1 Terabit/second [1, 2]. The millimeter waves (mmWaves) and terahertz have been approved for 5G and 6G systems respectively, the mmWaves range from 30 to 300 GHz and the terahertz range is 0.1–10 THz [3, 4]. One of the main challenges for the deployment of 5G/6G technologies is the spectrum to be adopted which means the necessary to investigate the channels' properties. In fact, mmWaves are adopted by 5G however, experiments to date have focused on frequencies below 100 GHz, the main work has been concentrated in bands below 60 GHz, or at most 95 GHz [5, 10]. On the other hand, the United States Federal Communications Commission (USFCC) advises the use of the bands from 95 GHz to 3 THz for 6G [11]. In such high-frequency bands, many researches are underway to reach extremely high data rates exceeding several Gbps. However, the mmWaves bands faces some propagation phenomena such as atmospheric absorption, penetration loss, human and building blockage, diffuse scattering from coarse materials, shadowing, refraction loss, and loss due to reflection. For the mmWaves propagation, the line of sight (LOS) can be predicted, while the non-LOS (NLOS) is also seen for the real obstacle.

In this paper, we considered several potential scenarios for analyzing mmWaves and sub-terahertz propagations at frequency bands of 28, 38, 60, 73, 100, and 120 GHz for outdoor Urban Microcell (UMi).

It is necessary to note that in the literature, various papers investigated mmWaves channels' properties using different scenarios but not in depth and ignoring the geometric parameters (Co-Pol/X-Pol, SISO/SIMO/MIMO) in the most recent works [5–7, 9, 10, 12] for outdoor UMi. Additionally, the effect of multi user–MIMO (MU–MIMO) on channels' properties did not taken into account by numerous researchers, as well as the effect of switching from LOS to NLOS scenarios on millimeter wave bands.

Compared with the existing studies, our key contributions in this work can be summarized as follows:

(1) An in-depth study of the propagation of different frequency bands using various scenarios was carried out, especially the geometric parameters (Co-Pol/X-Pol, SISO/SIMO/MIMO).

(2) The effect of Multi User MIMO (MU–MIMO) on the mmWaves channel characteristics mainly the impact of switching from 1U-MIMO to 2U-MIMO and 2U-MIMO to 4U-MIMO are discussed where in the literature the most researchers have not investigated this study.

(3) The effect of switching from LOS to NLOS.

(4) Focusing on the analysis of the propagation of frequency bands around 100 GHz (sub-terahertz) that are candidates for 6G systems, taking into account the potential scenarios with additional analysis and details.

The rest of this paper is structured as follows. Section I reviews several related works in which we present recent works studying propagations at mmWaves bands and enclose this section with a comparison with the contribution of this paper in terms of mmWave/terahertz bands, scenarios and reported parameters.

Section 2 reports 5G propagation problems and path loss models used in the existing works. In Section 3, we study the greatest candidate mmWaves and sub-terahertz channels (28, 38, 60, 73, 100, and 120 GHz) for different scenarios using the statistical spatial channel model NYUSIM [12], the results obtained can be used as a benchmark to illustrate different channel models in various scenarios for 5G/6G systems. Finally, Section 4 provides concluding remarks.

1. RELATED WORKS

The Radio propagation models have a significant impact on decisions made in the field of wireless communications that are developed to assist researchers in the deployment, design, study, and evaluation of various proposed wireless technology solutions. In [13], the authors developed a mathematical hypothesis to demonstrate the statistical performance of the field and the signals encountered in mobile radio communication in terms of a set of separated plane waves, redirected by a scattering and reflecting obstruction, and incident horizontally on the mobile radio reception via the Rayleigh fading channel. Exploiting the Rayleigh fading channel model pioneered by Clarke, Smith et al. in [14], developed simulation software for outdoor and indoor propagation channels.

Rappaport et al. in [15], developed another simulator named SIRCIM (Simulation of Indoor Radio Channel Impulse Response Models) for radio channel impulse response statistical models for the analysis and design of wireless communication systems. Fung et al. [16], developed another software simulation named Bit Error Rate Simulator (BERSIM) to evaluate in real time the link quality between a transmitter and receiver in mobile radio communication without resorting to any radio frequency equipment. Latest advances in the mmWaves communication area brought renewed interest to researchers in modeling 5G communication channels [5, 10]. In the literature, many path loss models are presented, but it is mandatory to know which ones are suitable for a given frequency range. The authors in [17], compared the performance of some path loss propagation models at mmWaves and terahertz frequencies which are the single frequency floating-intercept (FI) model, the single-frequency close-in (CI) model, the multi-frequency alpha-beta-gamma (ABG) model, and the multi-frequency close-in frequency dependent (CIF) model. Furthermore, the authors in [18], conducted a thorough review of channel models for the development of 5G radio frameworks, including the overall structure of channel models and the main distinctions among mmWaves and microwave channel models.

It is important to note that all frequency bands must be studied in different scenarios, in some work the survey was specified for a region or a city. The authors in [19], presented a data set for the propagation losses of wireless communications for the bands 28, 37, and 39 GHz for four major Indian cities, based on the corresponding weather conditions, in which the path losses take into account various atmospheric weather conditions. The channel characterization is most often performed in various urban areas, where both LOS and NLOS are considered. Otherwise, due to the scope of millimeter-wave channel modeling and the requirement to operate in frequency bands greater than 6 GHz for wireless communication such as 5G/6G, many groups of researches have begun to share their expertise to create mmWaves channel models and establish a performance evaluation platform. Among these groups, the NYU WIRELESS academic research center that developed NYUSIM model and finally simulation software adopted [12, 20].

The NYUSIM model [12] is based on the close-in (CI) model [3, 17] and on field measurements for several years in the 28 to 140 GHz range in New York City [20, 21]. NYUSIM model proves its performance in comparison with other models [18]. At New York University, Rappaport and his team developed a channel simulator named NYUSIM [22] for millimeter bands based on expanded real-world for channel propagation measurements. The simulator builds the real time channel response as well as the spatial channel response in order to properly evaluate the 5G physical and link layers. The mentioned model is based on the Statistical Spatial Channel Model (SSCM) involving Spatial Lobes (SL) and Time Clusters (TC) to get the corresponding Angle of Arrival (AoA) and Angle of Departure (AoD) of the power spectrum for the channel responses [23]. In addition, the model received the multi-path components in a time-cluster manner from different pointing angles by means of high-gain

Table 1. Some recent studies related to mmWave/terahertz frequency bands

Reference	Frequency channel	Scenario	Reported parameters
[5] 2020	27/39 GHz	MIMO	Gain, efficiency
[6] 2021	60 GHz	RT Outdoor by Ray Tarcing	Path Loss, Received Signal Strength
[7] 2020	Sub-6 GHz	Deep learning RT Outdoor	Spectral efficiency
[9] 2021	Sub-6 GHz/28 GHz		Session drop probability
[10] 2021	28/60 GHz	UMi Indoor	Path loss
[12] 2021	28/140 GHz	UMi LOS/NLOS indoor	Path Loss, RMS delay spread
[17] 2017	30/140/300 GHz	Indoor LOS	Path Loss, Path loss Exponent
[19] 2018	28/37/39 GHz	UMi Outdoor	Attenuation due to atmospheric gase, rain and fog
[26] 2019	28/38/60/73 GHz	UMi LOS Outdoor	PL, PLE, RMS Delay Spread
[27] 2019	25/28/38 GHz	Rain senario	PL
This paper	28/38/60/73/100/120 GHz	UMi LOS/NLOS, Polarisation (Co-Pol/X-Pol), Antenna patterns (SISO/SIMO/MIMO), users in MIMO configuration (MU-MIMO, Rain rate,Température /Humidity	PL, PLE, Received power, RMS Delay Spread

MIMO directional antennas. These features are not considered in WINNER [24] and 3GPP models [23]. Asma Ali Budalal et al. in [25], outlined the impacts of various weather events in tropical areas such as rain on the behavior of the millimeter-wave channel at the carrier frequency 38 GHz. Besides, the authors in [26], carried out a NYUSIM simulation of spatial channel modeling characteristics for 5G mmWaves at carrier frequencies (28, 38, 60, and 73 GHz). The authors in [27], investigated on the rainfall estimation of backhaul link using mmWaves frequencies (25, 28, and 38 GHz) in Beijing. Moreover, the impact of rain on mmWaves communications by an earthly path in tropical areas, is investigated in [28]. In [29], the impact of weather conditions on the channel model characteristics of millimeter wave band frequencies (60 and 73 GHz) considering the rainy season and winter season in Bangladesh is discussed. To assist in the modeling and design of the statistical channel model for future 5G and 6G mmWaves/sub-terahertz communications, the contribution of this article is twofold. First, using NYUSIM [12, 20] to provide a new statistical analysis of the effect of degraded environmental factors and number of users in MIMO configuration on channel characteristics of unlicensed 60 GHz and licensed 28, 38, and 73 GHz mmWaves frequencies and 0.1, 0.120 THz frequencies. Second, and more generally, we consider five scenarios for different channel parameters and antenna configurations.

Comparing our contributions with those of other recent works allows us to draw the conclusions outlined in Table 1. The comparison is made in terms of frequency bands, scenarios and reported parameters. It is easy to observe that the different scenarios adopted in this paper are polarization (Co-Pol/X-Pol), antenna patterns (SISO/SIMO/MIMO) and the number of users in MIMO configuration (MU-MIMO) as well as the reported parameters.

2. PATH LOSS MODELS

The Radio propagation models have a significant impact on decisions made in the field of wireless communications. The 5G/6G wireless communications offers tremendous promise, to the point where users can already expect to have access to ultra-high data rates from anywhere and at any time. However, these new communications are already subject to some criticism. Indeed, field tests have shown that this may only be true in optimal conditions, since 5G/6G systems operate on mmWaves and terahertz frequencies. Furthermore, 5G wireless communications can be severely affected by weather conditions, path loss (PL), attenuation due to atmospheric conditions, reflection loss, building materials, blocking of obstacles and scattering [19, 30].

Industry and academic researchers have attempted to develop competitive wireless technology, but they have been faced with an unprecedented demand for capacity and higher data rates. Therefore, it is necessary to use higher frequencies at 6 GHz and above 100 GHz for 5G/6G technologies. Thus, to optimize network efficiency and get more details on some candidate frequency bands for future mobile communication technology.

2.1. CI-Path Loss Model

Based on the NYUSIM platform [12, 20], this section investigates the path loss model, the strength of the received signal and power delay profiles.

2.1.1. Path loss. We consider the close-in free space (CI) reference distance path loss model with a reference distance of 1 m taking into account additional atmospheric attenuation factors in NYUSIM, expressed as follows [3, 22, 31]:

$$PL^{\mathrm{CI}}(f,d)[\mathrm{dB}] = FSPL(f,1\mathrm{m})[\mathrm{dB}] + 10n\log_{10}(d) + AT[\mathrm{dB}] + x_{\sigma}^{\mathrm{CI}}, \quad (1)$$

where $d \geq 1\mathrm{m}$, f indicates the carrier frequency in GHz, $d[\mathrm{m}]$ is the distance between the transmitter (TX) and the receiver (RX), n denotes the Path Loss Exponent (PLE), AT attenuation term caused by the atmosphere, x_{σ}^{CI} is a zero-mean Gaussian random variable with a standard deviation σ in dB, and $FSPL(f,1\mathrm{m})$ denotes the free space path loss in dB at the carrier frequency f at a TX-RX separation distance of 1m.

$$FSPL(f,1\mathrm{m})[\mathrm{dB}] = 10\log_{10}\left(\frac{4\pi f\times 10^{9}}{c}\right) = 32.4[\mathrm{dB}] + 20\log_{10}(f), \quad (2)$$

where c is the speed of light in a vacuum, of which f is in GHz. The term AF is considered by:

$$AT[\mathrm{dB}] = \alpha[\mathrm{dB/m}]\times d[\mathrm{m}], \quad (3)$$

where α is the attenuation factor in $\mathrm{dB/m}$, that illustrates the collective mitigation effect of water vapor fog, rain and dry air [31]. The parameter d is the 3D TX-RX separation distance in (1).

The PL caused by co-polarized (Co-Pol) TX and RX antennas is expressed as [32]:

$$PL_{V-V}(d) = P_{T-V} - P_{R-V} + G_T + G_R, \quad (4)$$

where P_{T-V} (dBm) is the transmitted power into the vertically polarized TX antenna, denotes the received power at the output of the vertically polarized RX antenna , G_T and G_R are TX and RX antennas gains (dBi) respectively.

The cross polarization (X-Pol) path loss PL_{V-H} is then calculated at the same distance as follows [32]:

$$PL_{V-H}(d) = P_{T-V} - P_{R-H} + G_T + G_R. \quad (5)$$

In the above equation, P_{R-H} is the power received at the output of the RX antenna horizontally polarized (dBm). X-Pol link involves transmitting in one polarization and receiving in the orthogonal polarization.

2.1.2 Received signal power. The received power is given as follows [31]:

$$\mathrm{P}_R[\mathrm{dBm}] = P_T[\mathrm{dBm}] + G_T[\mathrm{dB}] + G_R[\mathrm{dB}] - PL(d)[\mathrm{dB}], \quad (6)$$

where P_R, P_T, G_T, and G_R designate respectively the signal received power, the signal transmitted power, the gain of the transmitting and receiving antennas. Furthermore, $PL(d)$ represents the average path loss at separation distance d.

2.1.3 Power delay profile (PDP). To illustrate the omnidirectional power delay profile (OPDP), the impulse response of the omnidirectional channel can be derived by [33]:

$$h_{\mathrm{omni}}\left(t,\vec{\Theta},\vec{\varphi}\right) = \sum_{n=1}^{N}\sum_{m=1}^{Mn} a_{m,n}\exp(j\varphi_{m,n})\delta(t-\tau_{m,n}) \times \delta\left(\vec{\Theta}-\vec{\Theta}_{m,n}\right)\delta\left(\vec{\varphi}-\vec{\varphi}_{m,n}\right), \quad (7)$$

where: t is propagation time described by absolute form, $\vec{\Theta} = (\theta,\varphi)$ is vector features azimuth and elevation angles of departures which characterize TX, $\vec{\varphi} = (\theta,\varphi)$ is vector features azimuth and elevation angles of arrivals which characterize RX N, M_n is the time clusters (TCs) number and the cluster subpaths number, $a_{m,n}$ is the value of the mth is subpaths pertaining to the nth TCs, $\tau_{m,n}$ is the time delays angles, $\varphi_{m,n}$ is the propagation angles.

3. SIMULATION SCENARIOS, ANALYSIS AND DISCUSSION

Based on the CI model, we analyzed and compared the proposed millimeter wave and sub-terahertz channels: 28, 38, 60, 73, 100, and 120 GHz for different scenarios. In this context, we have considered different scenarios divided into two categories: First, the geometric parameters: Co-Pol/X-Pol, antenna patterns (SISO/SIMO/MIMO) and number of users in MIMO configuration (MU-MIMO). Second, the environmental conditions: LOS/NLOS, rain rate, temperature and humidity for an urban microcell. In this section, we use the NYUSIM model, which is shown to be more accurate for realistic simulations than other channel models in urban environments [20]. Unlike the 3GPP model [23], which relied on many legacy results below 6 GHz, NYUSIM emphasizes a more physical basis and relies on massive amounts of real data measured at mmWave frequencies [34]. Simulation parameters evoked in this section are summarized in Table 2. Furthermore, unless otherwise stated, we set the environment scenario to LOS.

Table 2. LOS/NLOS scenario parameters

Channel Parameters Value		Antenna Parameters	Value
RF Frequency	28/38/60/73/100/120 (GHz)	TX/RX Array Type	ULA/ULA (Uniform Linear Array)
RF BW, MHz	800	Num TX/RX Elements	1/1
Scenario	UMi	TX/RX Antenna Elements Spacing	0.5λ/0.5λ
Environment	LOS/NLOS	TX Azimuth/Elevation HPBW	10°/10°
T-R Separation, m	100	RX Azimuth/Elevation HPBW	10°/10°
TX Power, dBm	30		
Num RX	1		
Press, mbar	1013		
Hum, %	50		
Temp., C°	20		
Pol	Co-Pol		
D Foliage, m	0		
Rain rate, mm/h	0		

3.1. LOS/NLOS Scenario

For all considered channels, we consider the LOS and NLOS environments. In this scenario, we have two phases:

In the first phase, we set LOS or NLOS then we investigate the frequency bands. Figures 1–3, show the PL, received power, and PLE of both the directional power delay profile DPDP and OPDP in terms of frequency bands. In the case of LOS scenario, for DPDP, the 28 GHz channel has lower PL and PLE 102.8 dB, 2.1 respectively, whereas 73 and 120 GHz have the highest values (116.1 and 116.3 dB) and vice versa for the received power. For OPDP, the 28 GHz channel has lower PL 98.8 dB, while the 100 GHz channel has the lowest PLE (1.8) and the 60 and 120 GHz channels have the two highest values (110.8 and 112.7 dB) and conversely for received power.

In the case of NLOS situation, for DPDP/OPDP, the 38 and 73 GHz channels have a lower PL and PLE (120.5, 119.7 dB for PL and 2.8, 2.5 for PLE), whereas for 60 GHz, it has the two highest values (144.9 dB, 3.9) and conversely for the received power. Nevertheless, the 100 and 120 [GHz] channels have roughly similar statistics for PL, PLE, and received power, while still being better than the 60 GHz channel. The authors in [26] confirmed the above results for 28, 38, 60 and 73 GHz frequency bands.

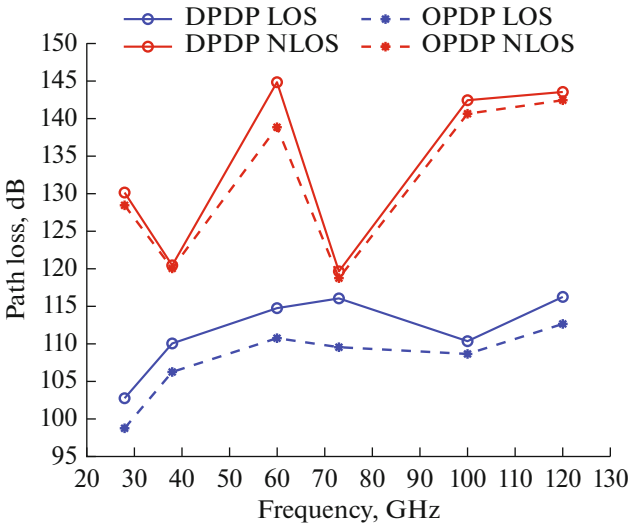

Fig. 1. Path loss for LOS/NLOS scenarios.

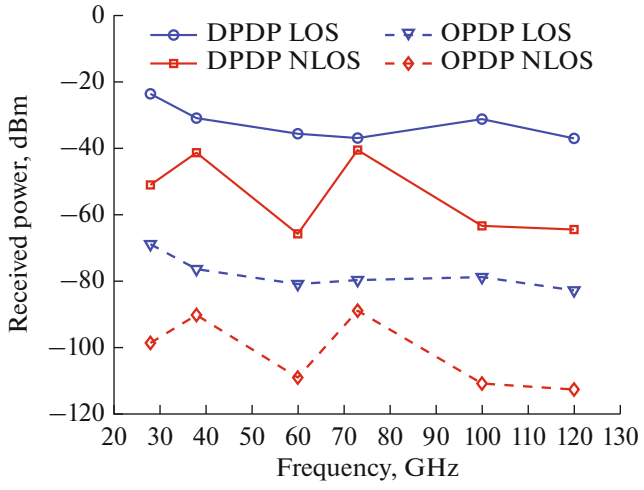

Fig. 2. Received Power for LOS/NLOS scenarios.

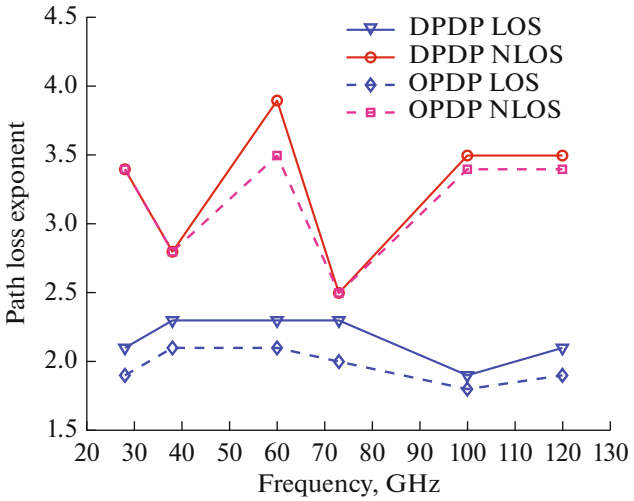

Fig. 3. Path Loss Exponent for LOS/NLOS scenarios.

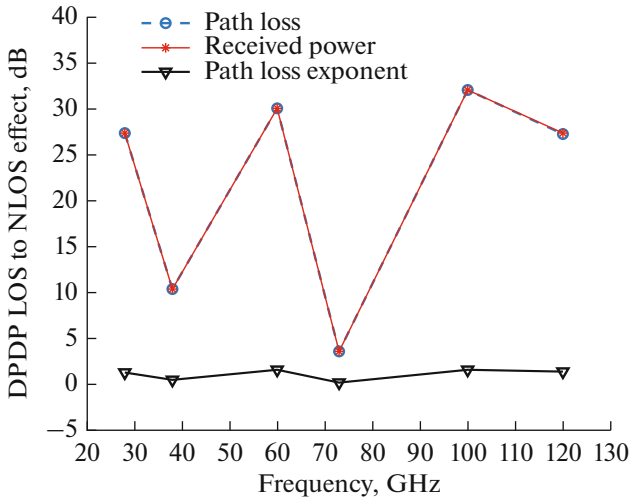

Fig. 4. Effect of changing the type of environment from LOS to NLOS on the characteristics of the channel for DPDP.

As a second phase, we investigate the impact of changing the type of environment from LOS to NLOS on the channel characteristics for DPDP and OPDP. Figures 4 and 5 show the effect of changing from LOS to NLOS situation on the characteristics of the channel for both DPDP and OPDP respectively. From these figures, we result that 100 GHz channel was widely affected by the change from LOS to NLOS (30 dB), besides the channel 73 GHz was less affected compared to the other channels (3 dB). While for 60 GHz, it has the two highest values and conversely for the received power (30 dB). Various works in the literature investigated the mentioned bands in LOS/NLOS scenarios but ignored the effect of changing from LOS to NLOS on channel characteristics as in [26, 35–38].

3.2. Co-Pol/X-Pol Scenario

Switching from Co-Pol to X-Pol (cross-polarization) can affect the channel characteristics and cause a significant path loss. The cross polarization discrimination (XPD) is determined by the difference between the path losses of the Co-Pol (V–V) and X-Pol (V–H) antenna. In this scenario we aim to study the polarization effect on the mentioned frequency bands (28, 38, 60, 73, 100, and 120 [GHz]).

Figures 6, 7 and 8, illustrate the PL, received power, and PLE of both DPDP and OPDP with LOS environment for Co-Pol/X-Pol polarizations. In case DPDP with Co-Pol polarization, the 28 GHz channel has a better PL and PLE (102.8 dB, 2.1), while 73 and 120 [GHz] have the two worsts values (116.1 and 116.3 dB 2.3, 2.1) and conversely for the received power.

For OPDP with Co-Pol polarization, the 28 GHz channel has the best PL 98.8 dB, while 120 GHz has the higher one 112.7 dB and conversely for the received power, 100 GHz has the lower PLE 1.8, whereas 38 and 60 [GHz] have the higher values 2.1. For DPDP and OPDP with X-Pol polarization, the 28 GHz has the lowest PL and the PLE (127.6 dB, 3.3), whereas, 120 GHz has the two higher values (146.2 dB, 3.6) and conversely for the received power.

The remaining channels show approximately the same statistics on their characteristics; however, the 73 GHz frequency demonstrates the greatest improvement.

Figures 9 and 10 show the impact of changing from Co-Pol state to the X-Pol on the characteristics of the channel for both DPDP and OPDP, respectively. From these figures, we can see that the 100 and 120 [GHz] channels are more affected by the change

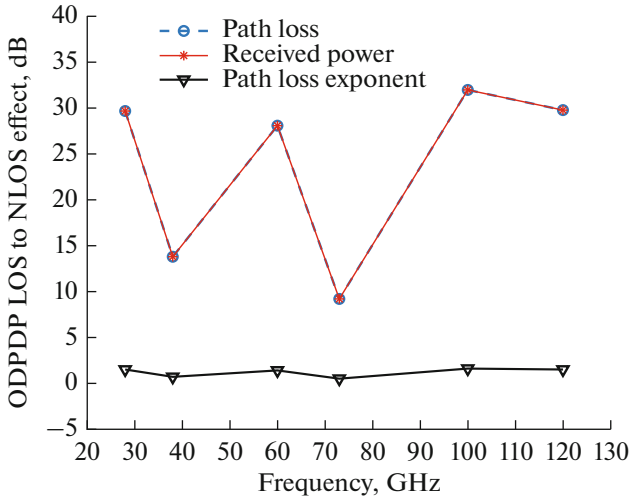

Fig. 5. Effect of changing the type of environment from LOS to NLOS on the characteristics of the channel for OPDP.

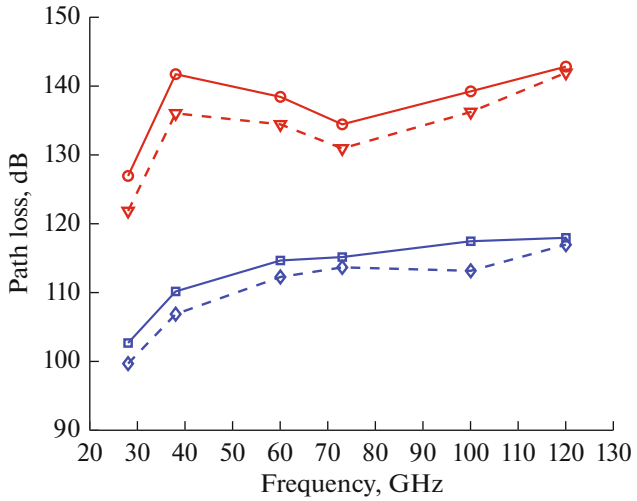

Fig. 6. Path Loss for Co-Pol/X-Pol scenario.

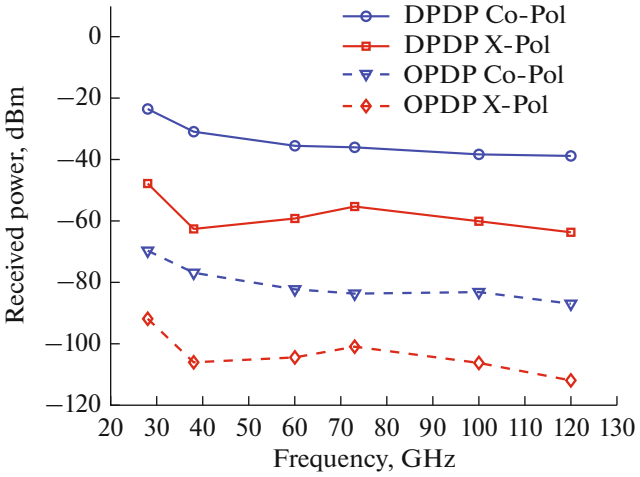

Fig. 7. Received Power for Co-Pol/X-Pol scenario.

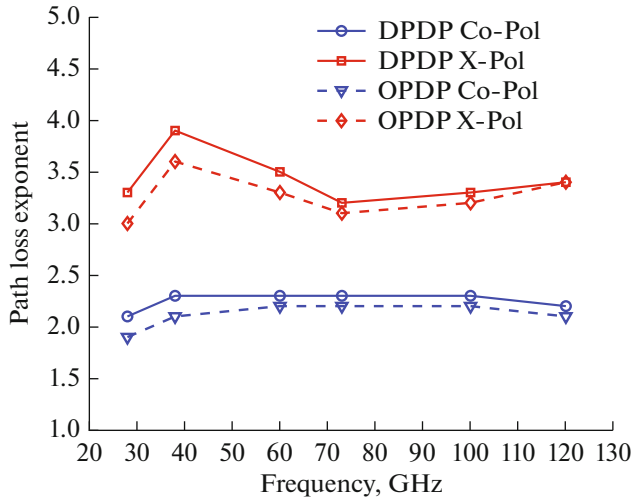

Fig. 8. Path Loss Exponent for Co-Pol/X-Pol scenario.

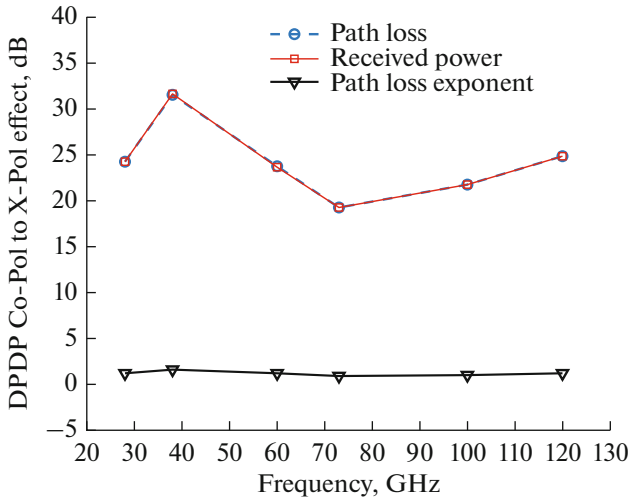

Fig. 9. Effect of changing from Co-Pol state to the X-Pol state on the characteristics of the channel for DPDP.

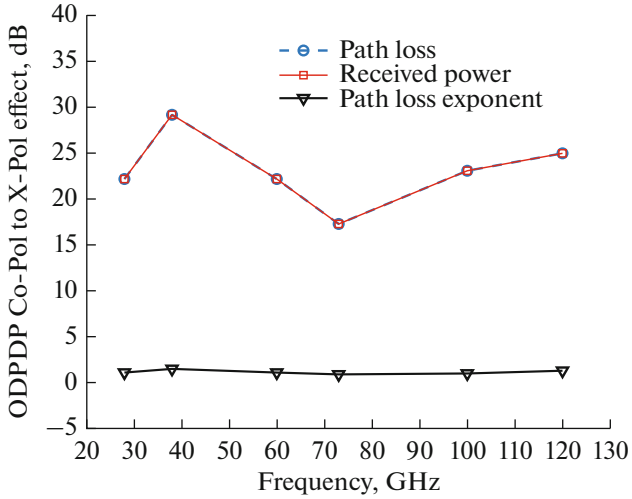

Fig. 10. Effect of changing from Co-Pol state to the X-Pol state on the characteristics of the channel for OPDP.

from Co-Pol to X-Pol on PL and received power (XPD = 30 dB). However, the 60 and 73 [GHz] channels experience lesser effects compared to the other channels (XPD = 22 dB). In addition, it is noted that all channels have approximately the similar impact on the PLE. Concerning the comparison with some works of the literature. In [39], the results indicate that the polarization effect on the mmWave communication channel at 73 GHz is much significant than 28 GHz. In this paper, the results indicate the opposite, where the effect depends on TX-RX separation distance (near field and far field). Otherwise, in [40], the authors given a comparison of cross-polarization at 28, 73, and 140 GHz for indoor scenario. The results showed that the XPD was constant over the T-R separation distance range from 3 to 6 m. We conclude that the range above 100 m, the outcomes are different

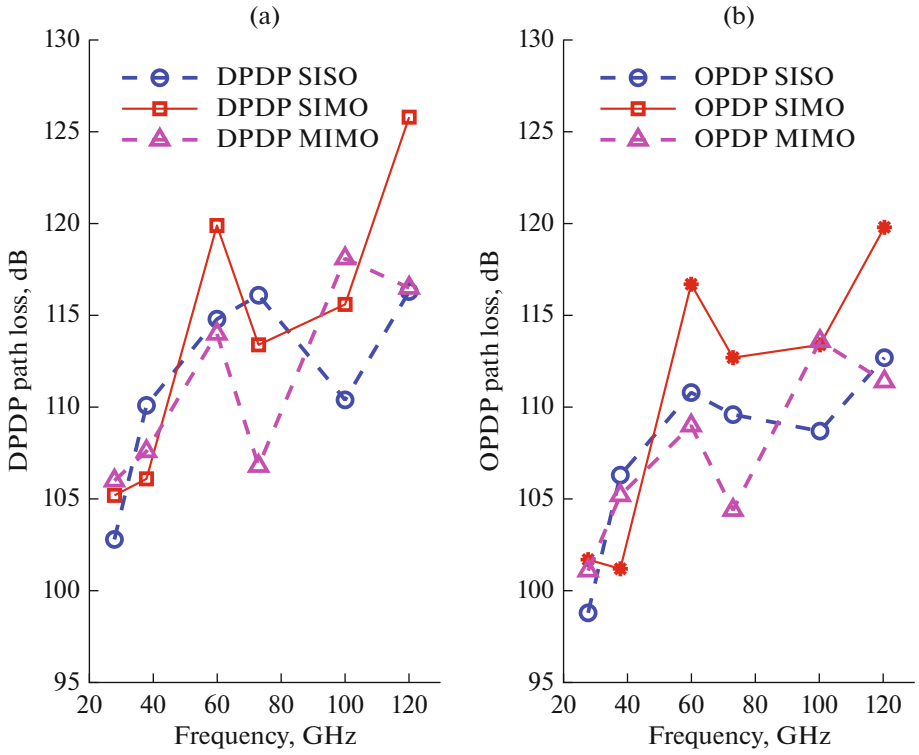

Fig. 11. Path Loss for SISO scenario in the case of: (a) DPDP, (b) OPDP.

where the value of XPD depended on the separation distance.

3.3. Antennas Patterns Scenarios

Here, we consider three antenna configurations as: SISO (1 × 1), SIMO (1 × 4) and MIMO (4 × 4).

Figures 11, 12 and 13, show the PL, received power and PLE of both DPDP and OPDP for SISO/SIMO/MIMO configurations.

For the SISO configuration, the 28 GHz channel exhibits a lower PL (102.8 dB), while the 73 and 120 [GHz] channels have the highest values (116.1 and 116.3 dB), and conversely for the received power. In addition, the 100 GHz channel shows a lower PLE (1.9), whereas the 38 GHz channel shows the higher one (2.3). In SIMO mode, channels 28 and 38 [GHz] have the lowest PL (105.2, 106.1 dB), meanwhile the channel 120 GHz has the highest value (125.8 dB), and conversely for the received power. In the end, the channel 38 GHz has the lowest PLE (2.1), while channels 60 and 120 [GHz] have the highest values (2.6). In the MIMO configuration, the 28 and 38 [GHz] channels have the lowest PL (106 , 107.6 dB), while the 100 and 120 [GHz] channels have the highest values (118.1, 116.5 dB) and conversely for the received power. In addition, channel 73 GHz has the lowest PLE (1.9), while channel 60 and 100 [GHz] have the highest values (2.3).

Figures 14 and 15 show the impact of switching from SISO to SIMO and SIMO to MIMO configuration on the channel characteristics for DPDP and OPDP, respectively. From Fig. 14, the 120 and 38 [GHz] channels are more affected by the transition from a SISO to SIMO channel on the PL and received power; however, respectively in the negative and positive way (variation of 9.5 dB and 4 dB respectively), while the 28 GHz channel is less affected compared to the other channels (2.4 dB). Furthermore, all channels have nearly a similar impact on the PLE.

It can be seen from Fig. 15 that the 120 and 73 [GHz] channels are most positively affected by the transition from a SIMO to a MIMO channel regarding to PL and received power (9.3 and 6.6 dB respectively), whereas the 28 GHz channel is less affected compared to the other channels (0.8 dB). All channels have approximately the same effect on the PLE. In [41], a proper selection of a number of antenna elements in 28 GHz frequency in NLOS and LOS environment and their performance is presented, by analyzing different channel parameters in urban microcell scenario for Dhaka city. The results indicate that the MIMO with a 4 × 4 antenna element is giving less path loss, better-received power and less RMS delay spread in comparison with other MIMO (2 × 2, 3 × 3, 5 × 5, 6 × 6, and 7 × 7). In our case, we confirm the results of 4 × 4 MIMO for 28 GHz, but for the others carriers

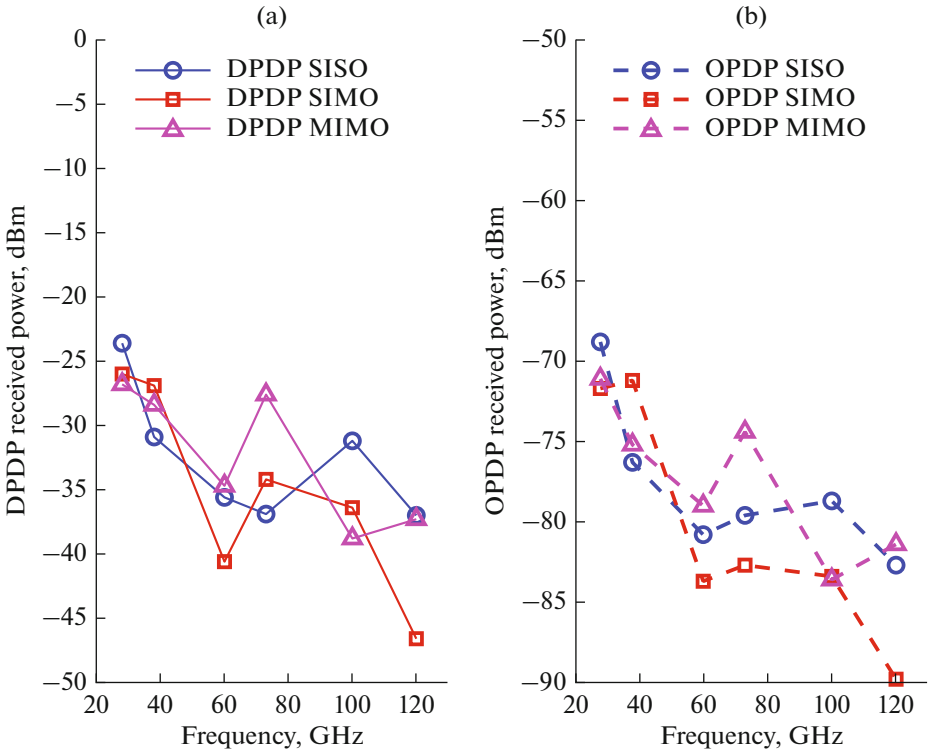

Fig. 12. Received Power for SIMO scenario in the case of: (a) DPDP, (b) OPDP.

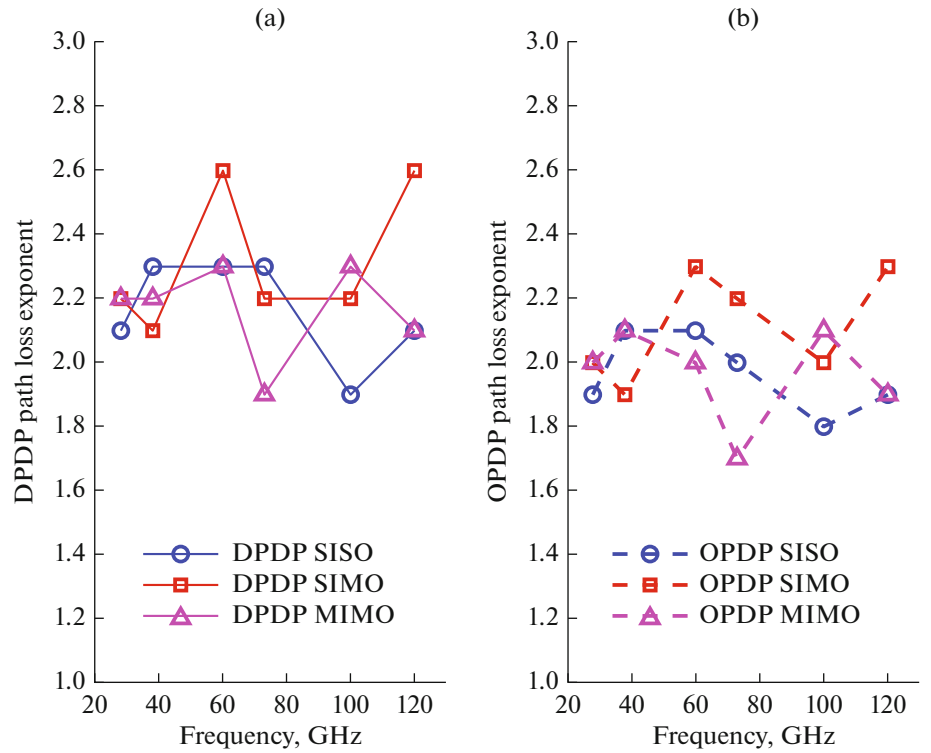

Fig. 13. Path Loss Exponent for MIMO scenario in the case of: (a) DPDP, (b) OPDP.

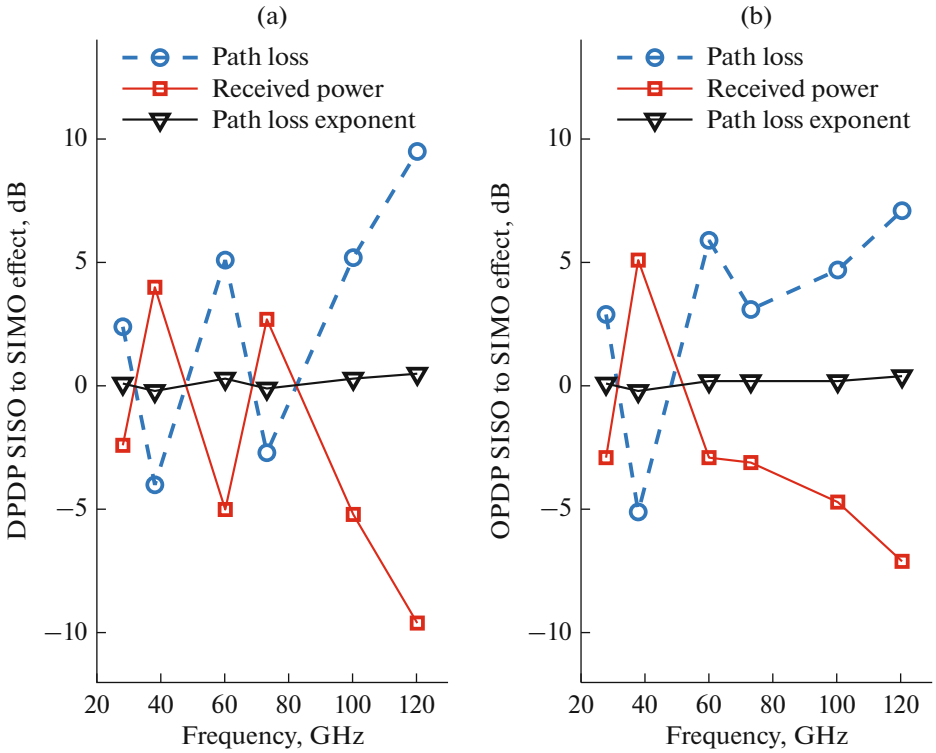

Fig. 14. Effect of changing from SISO to SIMO channel for: (a) DPDP, (b) OPDP.

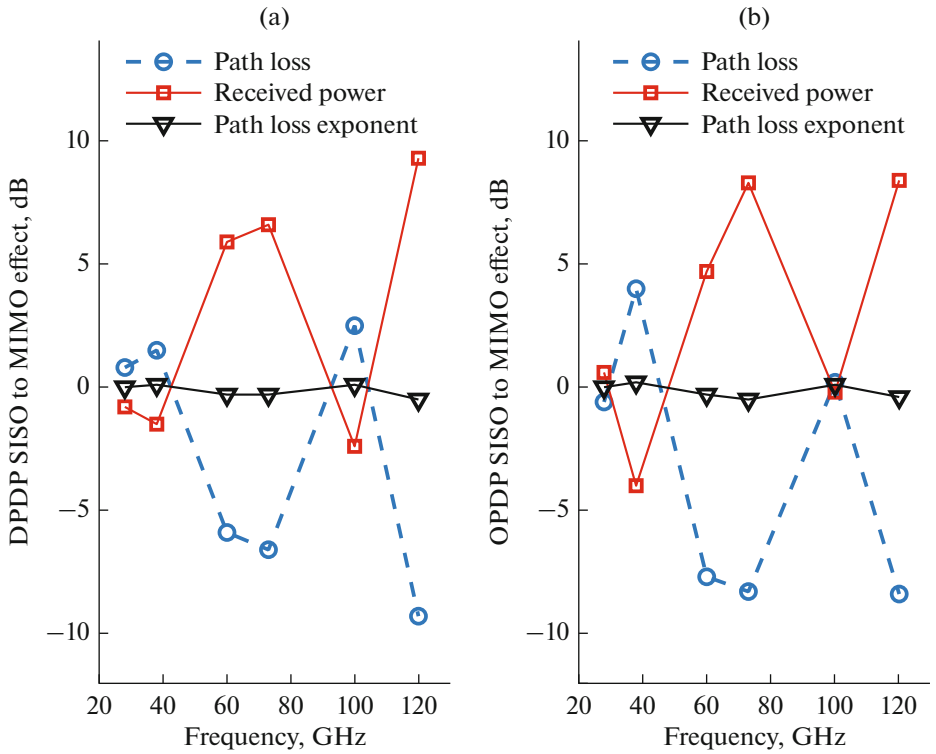

Fig. 15. Effect of changing from SIMO to MIMO channel for: (a) DPDP, (b) OPDP.

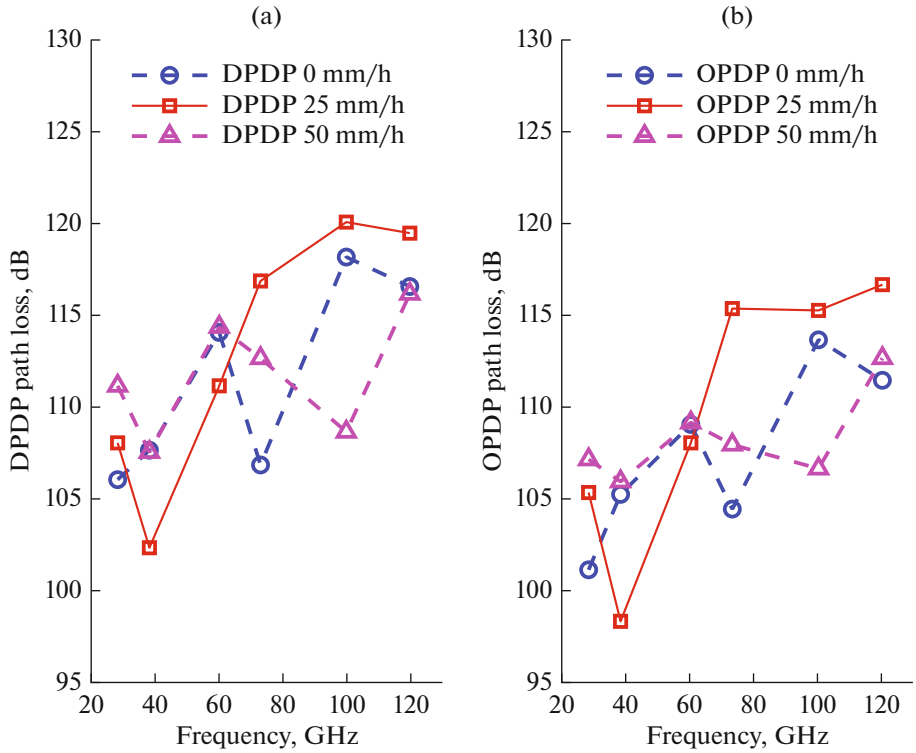

Fig. 16. Path Loss for rain scenario in the case of: (a) DPDP, (b) OPDP.

frequencies (38, 60, 73, 100 and 120 GHz) are not conducted.

3.4. Rain Scenario

We consider the rain scenario with three precipitation rates: 0, 25 and 50 mm/h. Figures 16, 17 and 18 show, the PL, received power, and PLE of both DPDP and OPDP for rain rate scenarios.

Based on these figures, for 0 mm/h rain rate setting, the 28 GHz channel has a lower PL (106 dB), while 100 and 120 [GHz] have higher values (118.1 and 116.5 dB respectively) and conversely for the received power. The 73 GHz channel has a lower PLE (1.9), while 100 GHz has the higher one (2.3). At 25 mm/h rain rate setting, the 38 GHz channel has the lower PL (102.3 dB), while 100 and 120 GHz channels have the higher values (120 and 119.4 dB respectively) and conversely for the received power. Moreover, the 38 GHz channel has the lower PLE (1.9), while 73 and 100 GHz have the higher value (2.4). In the case of 50 mm/h rain rate setting, the 38 GHz channel has the lower PL (107.5 dB), while the 120 GHz channel shows the higher one (116.1 dB) and conversely for the received power, the 100 GHz channel holds the lower PLE (1.8), while 28 GHz has the highest value (2.5).

Figures 19 and 20 show the impact of changing from 0 to 25 mm/h rain rate and from 25 to 50 mm/h rain rate on channel characteristics for both DPDP and OPDP, respectively. From Fig. 19, the 73 and 38 [GHz] channels are more affected by the change from 0 to 25 mm/h rain rate on PL and received power, however, respectively in the negative and positive way (10 dB, 5.3 dB respectively) while channels 60 and 100 [GHz] less affected compare to the other channels (2.9 dB, 1.9 dB respectively). Overall, all channels have approximately the same effect on PLE (between 0.1 and 0.2). Similarly, from Fig. 20, the 73 and 100 [GHz] channels are most adversely affected by the change from 25 to 50 mm/h rain rate on PL and received power (4.2, 11.4 dB respectively), while the 28 and 60 GHz channels are the least affected (3.1, 3.2 dB respectively). In addition, a similar impact on PLE was observed for all channels.

In [19], the results obtained indicate that with an increase in the carrier frequency, the attenuation level increases. The rain fade increase by 7 dB with a variation of the frequency from 28 GHz to 37 GHz. Compared to our outcomming the attenuations increase rapidly for the frequencies 60 to 73 [GHz] by 13 dB, whereas 2 dB with a variation of frequencies from 28 to 38 [GHz] as shown in Figs. 19 and 20. This difference depend to the setting parameters of the channel radio link.

In [42], a brief analysis of rain fading was presented based on the simultaneous measurement of one-minute rain rate and its effects on a short experimental link of 38 GHz. Rain fade average is observed as high as

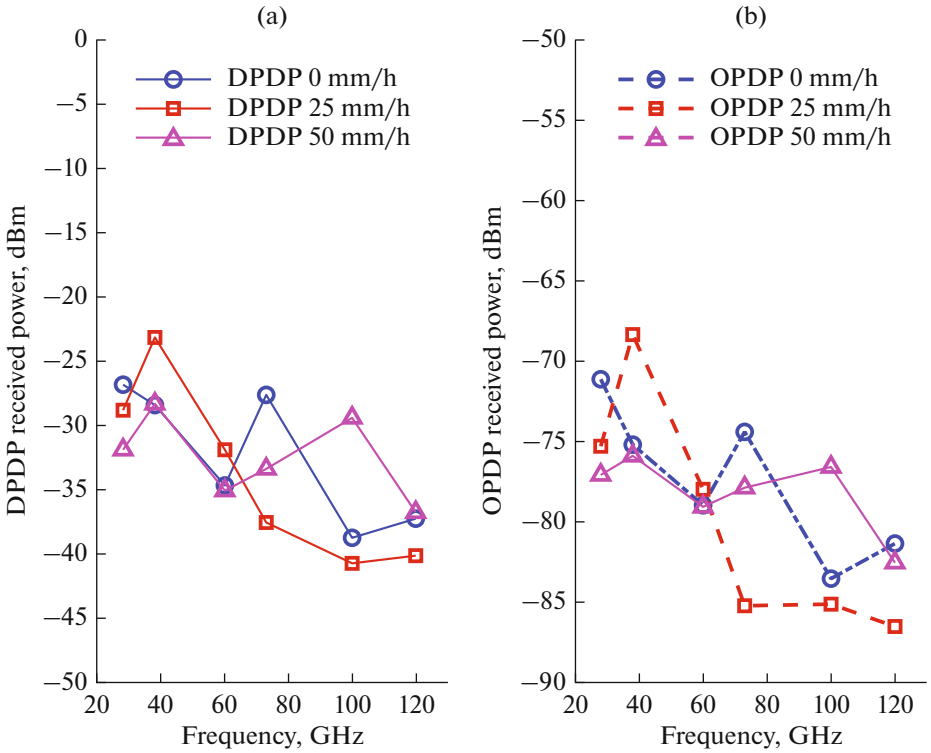

Fig. 17. Received Power for rain scenario in the case of: (a) DPDP, (b) OPDP.

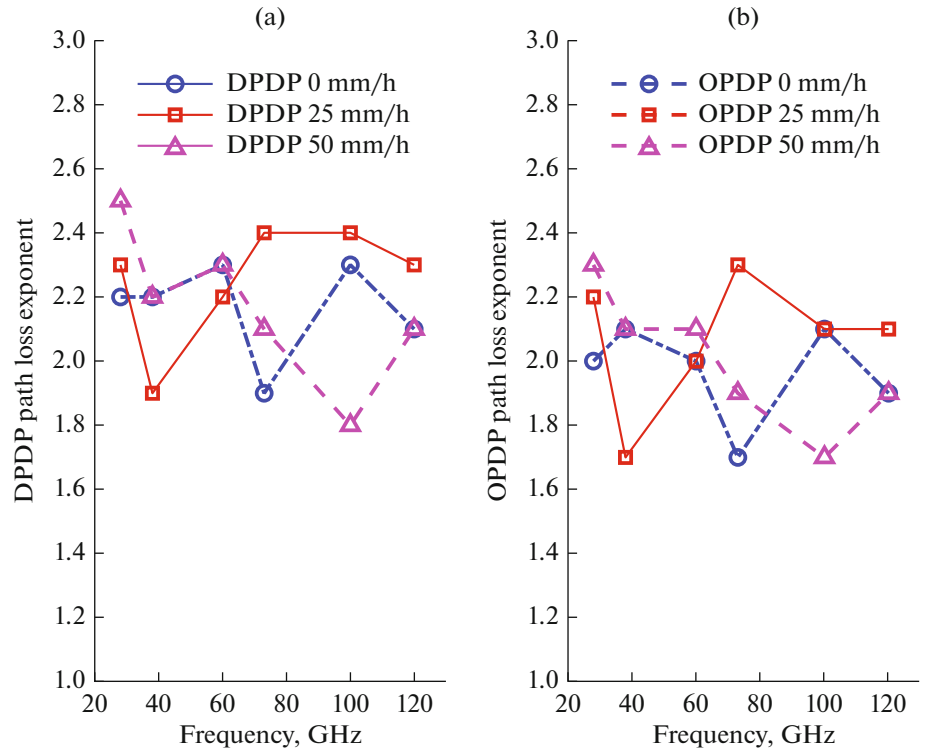

Fig. 18. Path Loss Exponent for rain scenario in the case of: (a) DPDP, (b) OPDP.

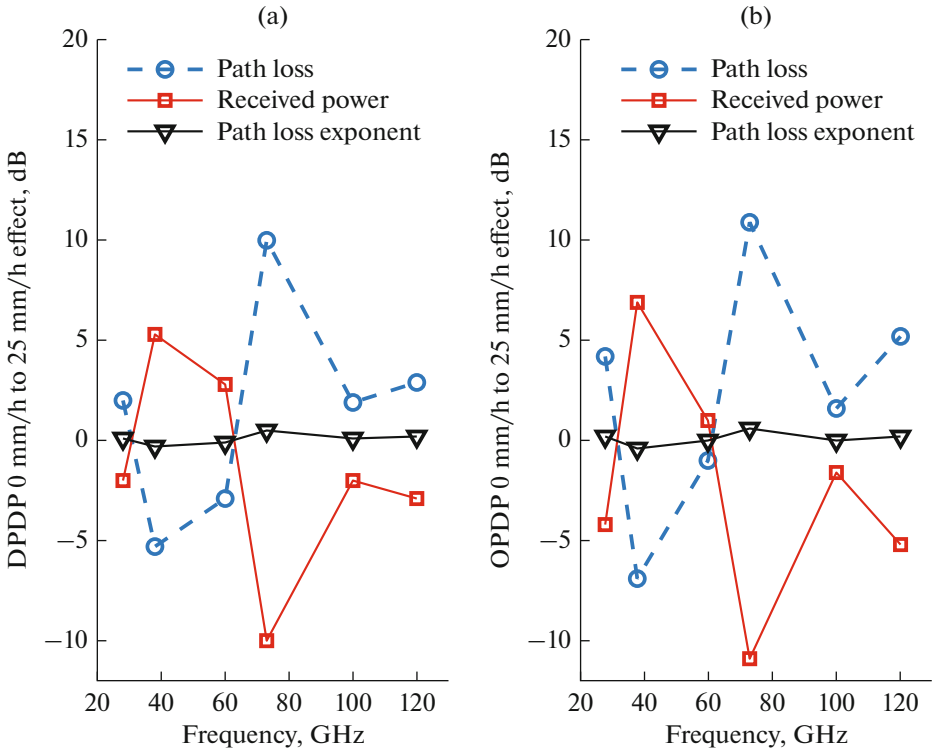

Fig. 19. Effect of changing from 0 to 25 mm/h rain rate on channel characteristics for: (a) DPDP, (b) OPDP.

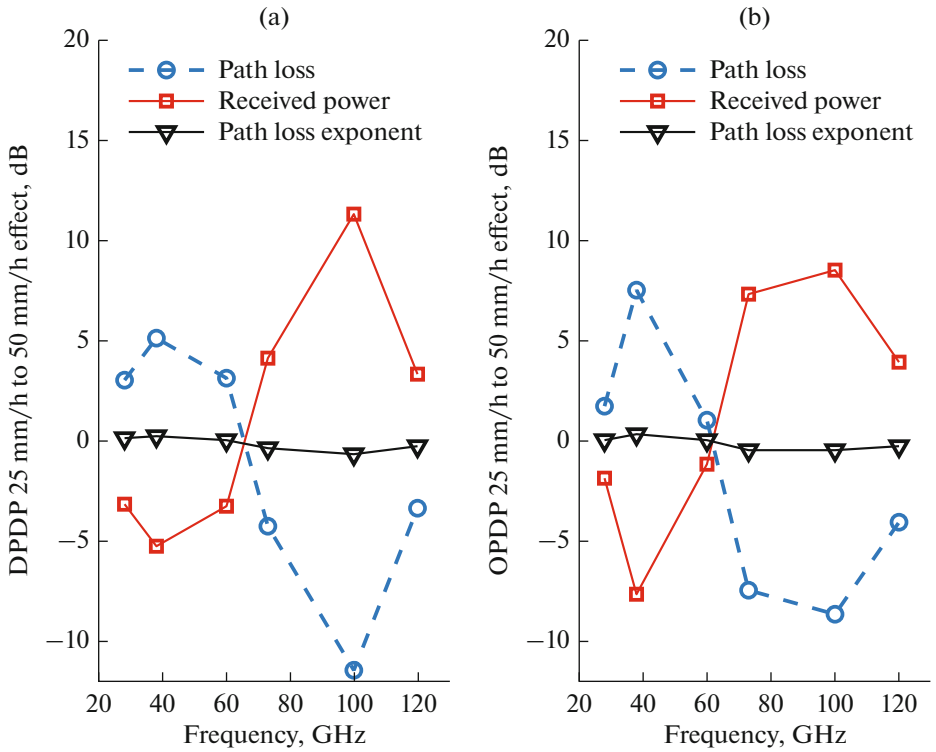

Fig. 20. Effect of changing from 25 to 50 mm/h rain rate on channel characteristics for: (a) DPDP, (b) OPDP.

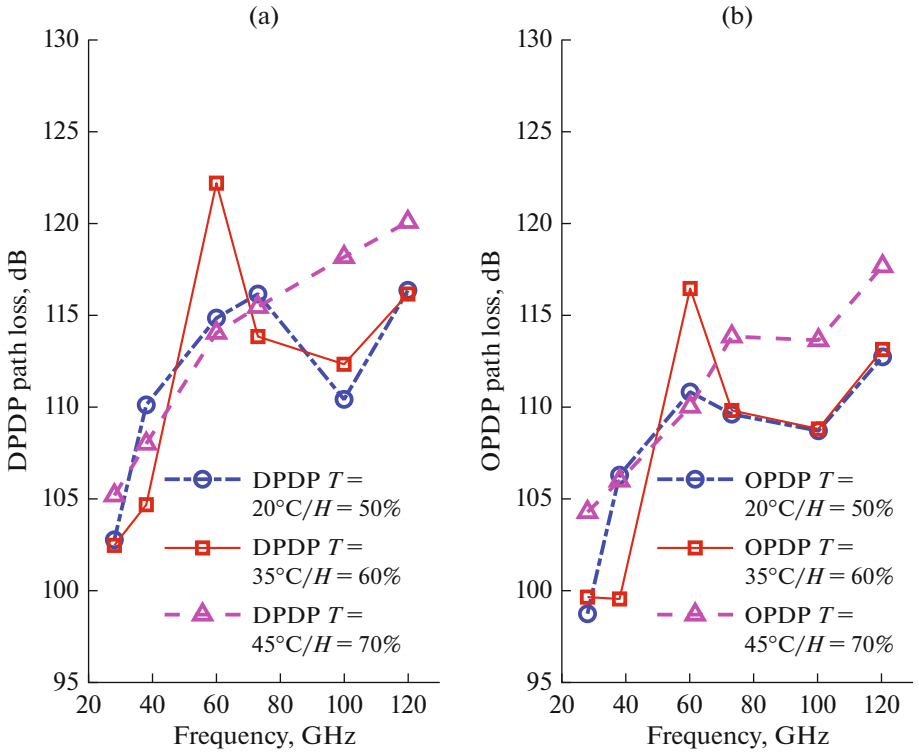

Fig. 21. Path Loss in case of temperature and humidity scenarios for DPDP and OPDP.

6.72 dB for 300 m path at about 30 mm/h rain intensity. In comparison with our results shown in Figs. 19 and 20, the rain fade is 5 dB for 100 m path with 25 mm/h rain rate variation, besides for 28, 60, 73, 100 and 120 GHz the rain fade are 2, 3, 10, 2 and 3 dB respectively.

3.5. Temperature and Humidity Scenario

In this scenario, we adopt three temperature and humidity values:

$$T1 = 20^{\circ}\text{C}/H1 = 50\%,\quad T2 = 35^{\circ}\text{C}/H2 = 60\%,$$
$$\text{and } T3 = 45^{\circ}\text{C}/H3 = 70\%.$$

Figures 21, 22 and 23 show the PL, received power, and PLE of both DPDP and OPDP for temperature and humidity scenarios.

(1) For $T1 = 20^{\circ}\text{C}/H1 = 50\%$ scenario, the 28 GHz channel has a lower PL (102.8 dB), while 60 and 120 [GHz] have higher values (114.8, 116.3 dB respectively) and conversely for the received power. For the 100 GHz channel, it has a lower PLE (1.9), while 38, 60 and 73 [GHz] channels have the higher values (2.3).

(2) For $T2 = 35^{\circ}\text{C}/H2 = 60\%$ scenario, the 28 and 38 [GHz] channels have a lower PL (102.5 dB, 104.7 dB respectively), while 60 GHz has the higher value (122.1 dB) and conversely for the received power. Channel 60 GHz has a higher PLE (2.7), while 38 and 100 [GHz] have the lower values (2).

(3) For $T3 = 45^{\circ}\text{C}/H3 = 70\%$ scenario, 120 GHz has the highest PL value (120 dB) whereas the 28 GHz channel has the lower PL (105.2 dB) and conversely for the received power. Channel 38 GHz has a low PL and high Received power compare to the others channels. All Channels have roughly the same value of PLE about (2.3).

Figures 24 and 25 show the impact of changing the weather condition from $T1 = 20^{\circ}\text{C}/H1 = 50\%$ to $T2 = 35^{\circ}\text{C}/H2 = 60\%$ and from $T2 = 35^{\circ}\text{C}/H2 = 60\%$ to $T3 = 45^{\circ}\text{C}/H3 = 70\%$ on channel characteristics for both DPDP and OPDP, respectively.

From Fig. 24, channel 38 [GHz] is more affected positively (variation of 5.4 dB) by the change from $T1 = 20^{\circ}\text{C}/H1 = 50\%$ to $T2 = 35^{\circ}\text{C}/H2 = 60\%$ on PL and received power; however, channel 60 [GHz] is more affected negatively (variation of 7.3 dB); while the other channels have roughly the same effect (variation of 2 dB). Furthermore, Fig. 25 reveals that 38 and 100 [GHz] channels are more adversely affected by $T2 = 35^{\circ}\text{C}/H2 = 60\%$ to $T3 = 45^{\circ}\text{C}/H3 = 70\%$, while 60 GHz channels are more positively affected on PL and received power (8.1 dB), while 28 and 73 GHz channels are less affected compared to other channels (about 2 dB). The same effect is observed on the PLE for all channels.

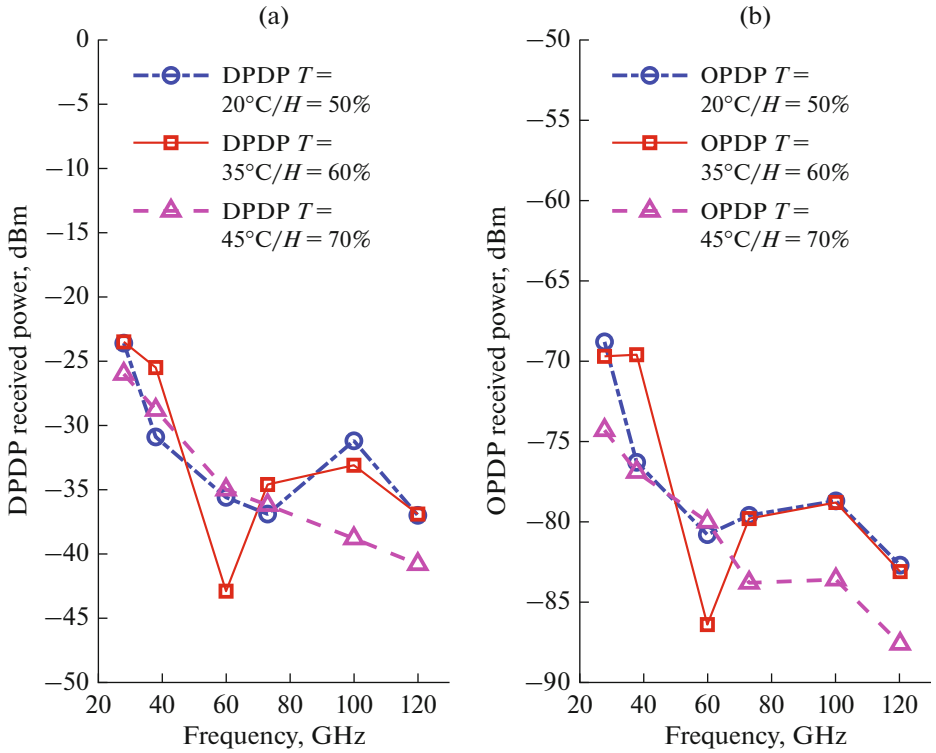

Fig. 22. Received Power in case of temperature and humidity scenarios for: (a) DPDP, (b) OPDP.

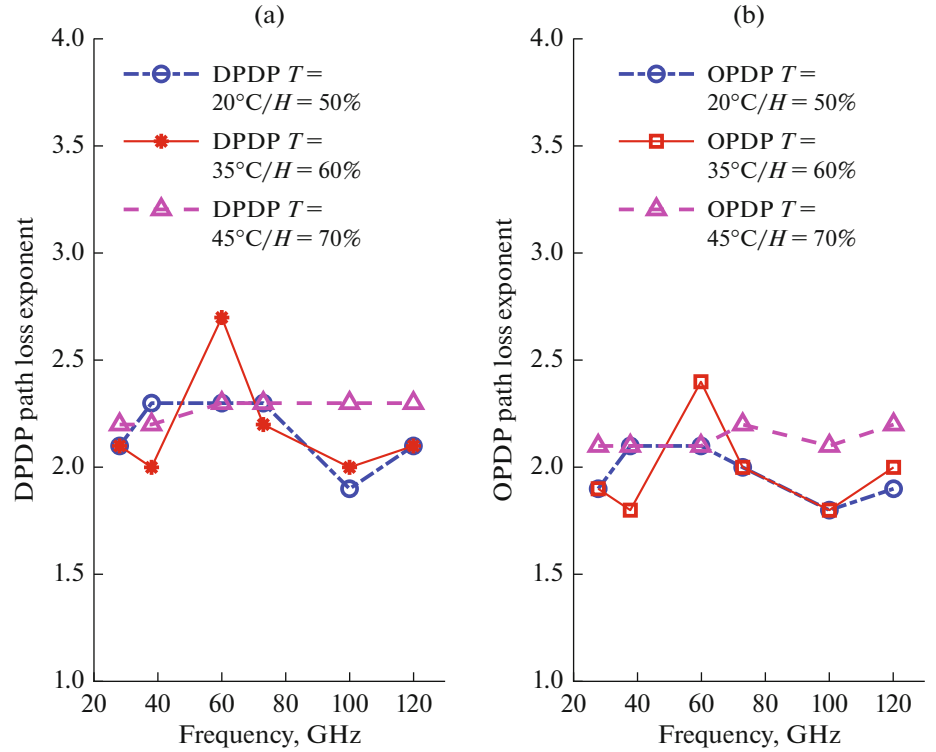

Fig. 23. Path Loss Exponent in case of temperature and humidity scenarios for: (a) DPDP, (b) OPDP.

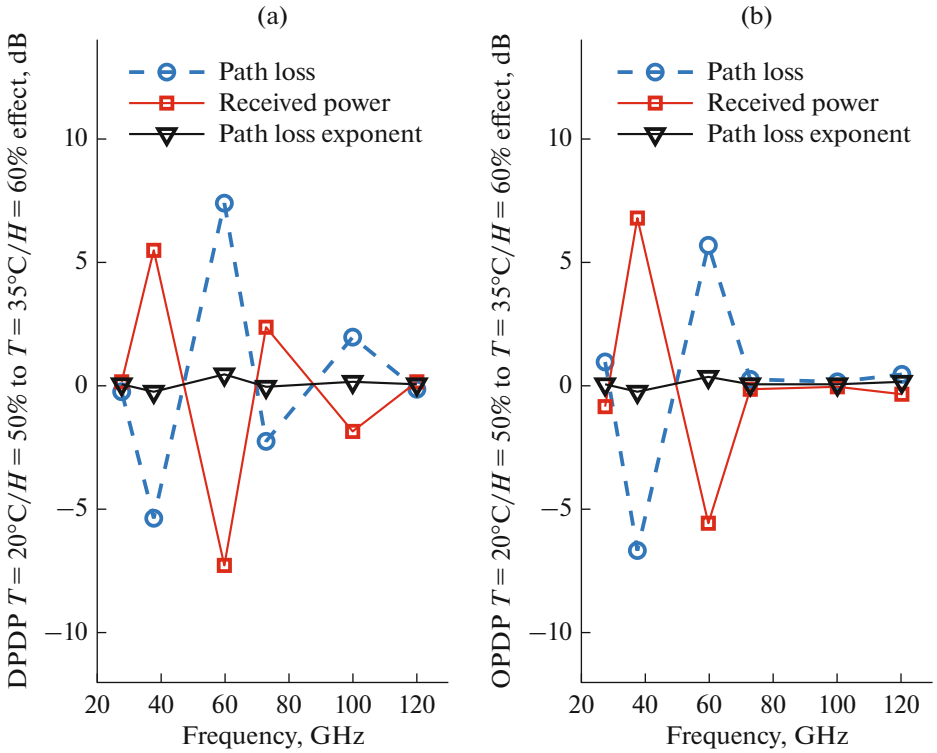

Fig. 24. Effect of changing of the weather condition from $T1 = 20°C/H1 = 50\%$, $T2 = 35°C/H2 = 60\%$ on channel characteristics for: (a) DPDP, (b) OPDP.

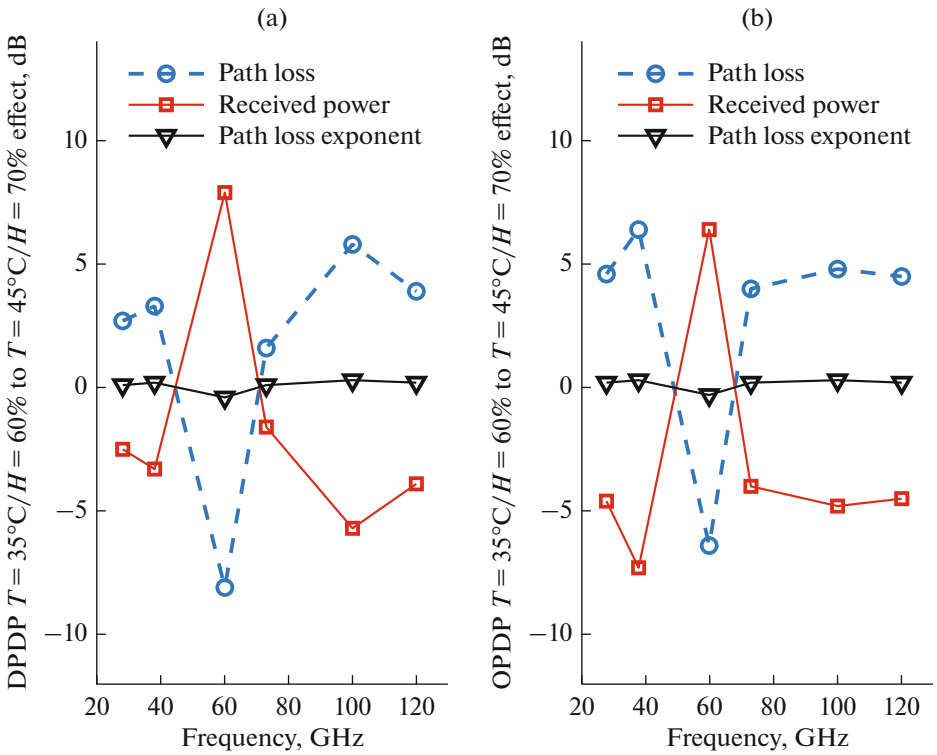

Fig. 25. Effect of changing of the weather condition from $T2 = 35°C/H2 = 60\%$ to $T3 = 45°C/H3 = 70\%$ on channel characteristics for: (a) DPDP, (b) OPDP.

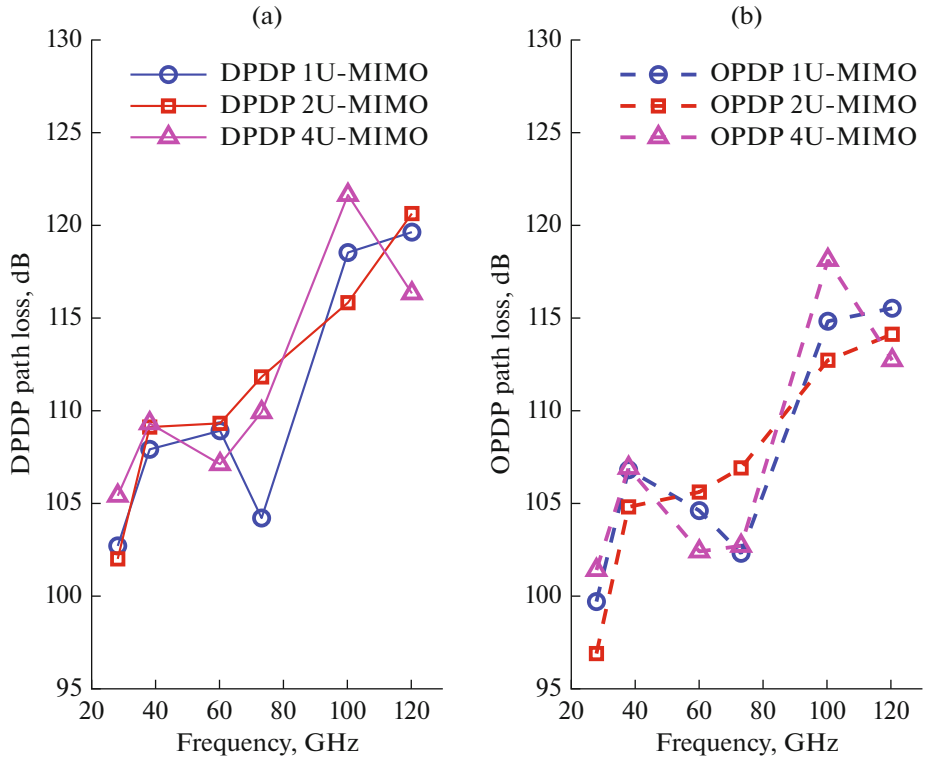

Fig. 26. Path Loss for MU-MIMO scenario in the case of: (a) DPDP, (b) OPDP.

In [43], the authors developed a custom model via the generic NYUSIM channel simulator, that fits the properties of mmWave propagation in Iraq environment and also the effect of weather parameters, as temperature and humidity, on link quality is discussed. The results indicate that a rise in the value of humidity causes a "concavity" in the 28 GHz subband performance while it has weaker impacts on the remaining bands especially for moderate values of humidity. In comparison with our results, the 38 and 60 GHz are more affected by the variation of the humidity and the temperature.

3.6. Multi User-MIMO Scenario

The evaluation of millimeter wave channels performance considering Multi User-MIMO (MU-MIMO) are ignored in the literature. In this last scenario, we consider three MU-MIMO configurations: 1U-MIMO (2 × 2), 2U-MIMO (2 × 2) and 4U-MIMO (2 × 2).

Figures 26, 27 and 28, show the PL, received power and PLE of both DPDP and OPDP for 1U-MIMO (2 × 2), 2U-MIMO (2 × 2) and 4U-MIMO (2 × 2) configurations.

For the 1U-MIMO configuration, the 28 GHz channel exhibits a lower PL 102.7 dB, while the 100 and 120 [GHz] channels have the highest values 118.5 and 119.6 dB respectively and conversely for the received power. In addition, the 73 GHz channel shows a lower PLE 1.6, whereas the 38, 100 and 120 GHz channels shows the higher one 2.1. In 2U-MIMO mode, channel 28 GHz has the lowest PL 102 dB, meanwhile the channel 120 GHz has the highest value 125.8 dB, and conversely for the received power. In the end, the channel 28 GHz has the lowest PLE 2, while channels 100 and 120 [GHz] have the highest values 2.2 and 2.6 respectively. In the 4U-MIMO configuration, the 28, 60 and 73 GHz channels have the lowest PL 105.4, 107.1 and 109.9 dB respectively, while the 100 and 120 GHz channels have the highest values 121.6 and 116.3 dB respectively and conversely for the received power. In addition, channel 73 GHz has the lowest PLE 2, while channel 100 GHz has the highest value 2.5.

Figures 29 and 30 show the impact of switching from 1U-MIMO to 2U-MIMO and 2U-MIMO to 4U-MIMO configuration on the channel characteristics for DPDP and OPDP, respectively. From Fig. 29, the 73 GHz is attenuated more than the other channels when switching from 1U-MIMO to 2U-MIMO (variation of 7.6 dB), while the 60 GHz channel is less affected (variation of 0.4 dB) compared to the other channels. Furthermore, all channels have nearly a similar impact on the PLE (0.1).

It can be seen from Fig. 30 that the 60 and 73 GHz channels are most positively affected by the transition from 2U-MIMO to 4U-MIMO channel in terms of

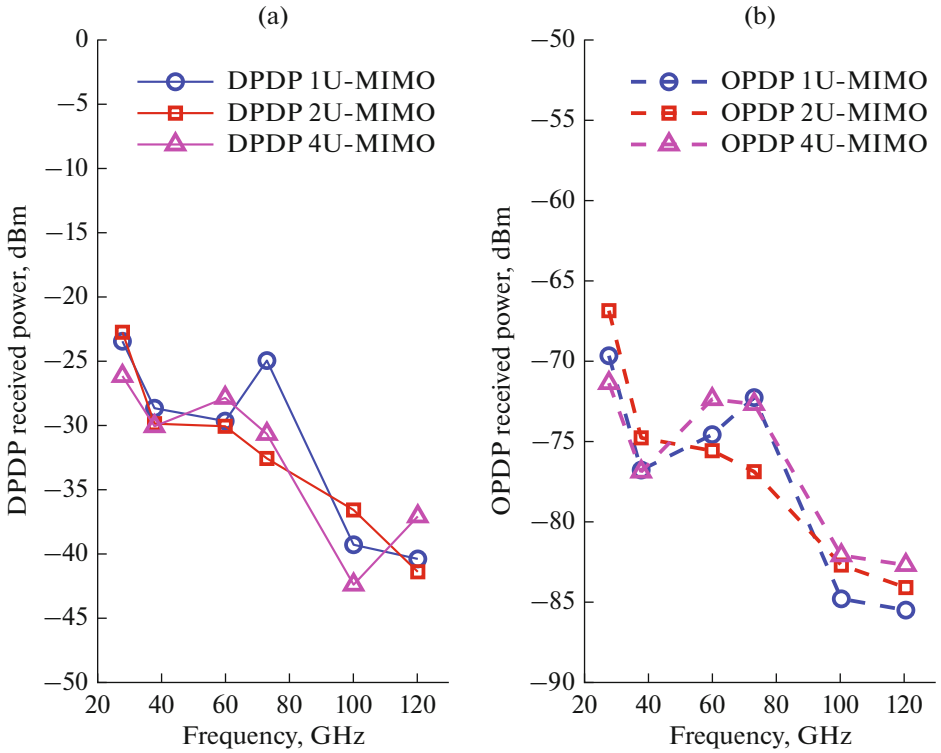

Fig. 27. Received Power for MU-MIMO scenario in the case of: (a) DPDP, (b) OPDP.

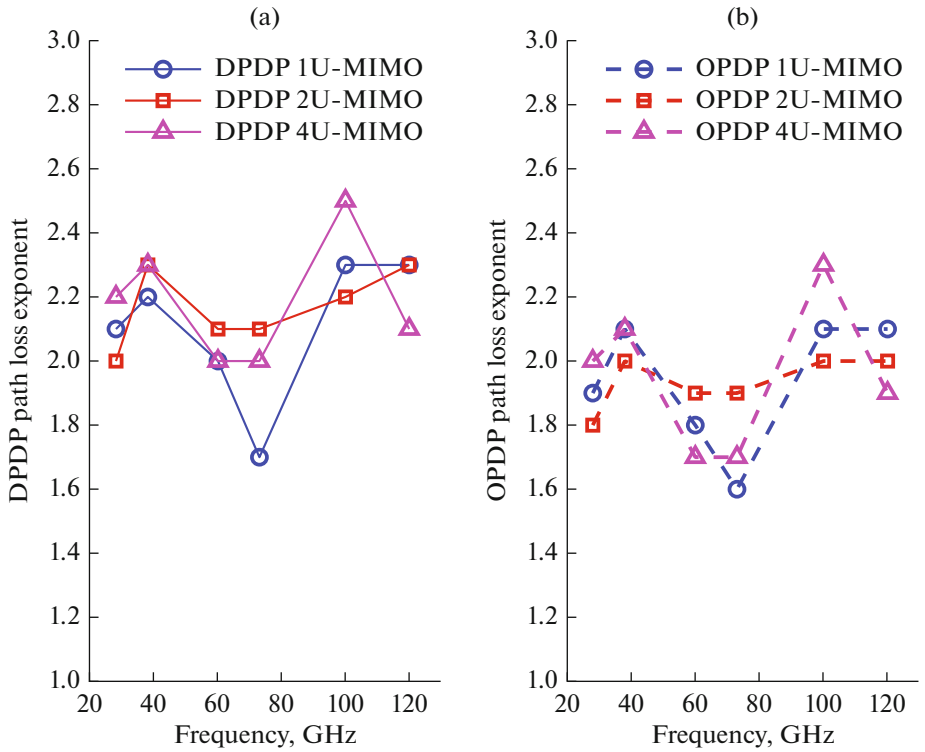

Fig. 28. Path Loss Exponent for MU-MIMO scenario in the case of: (a) DPDP, (b) OPDP.

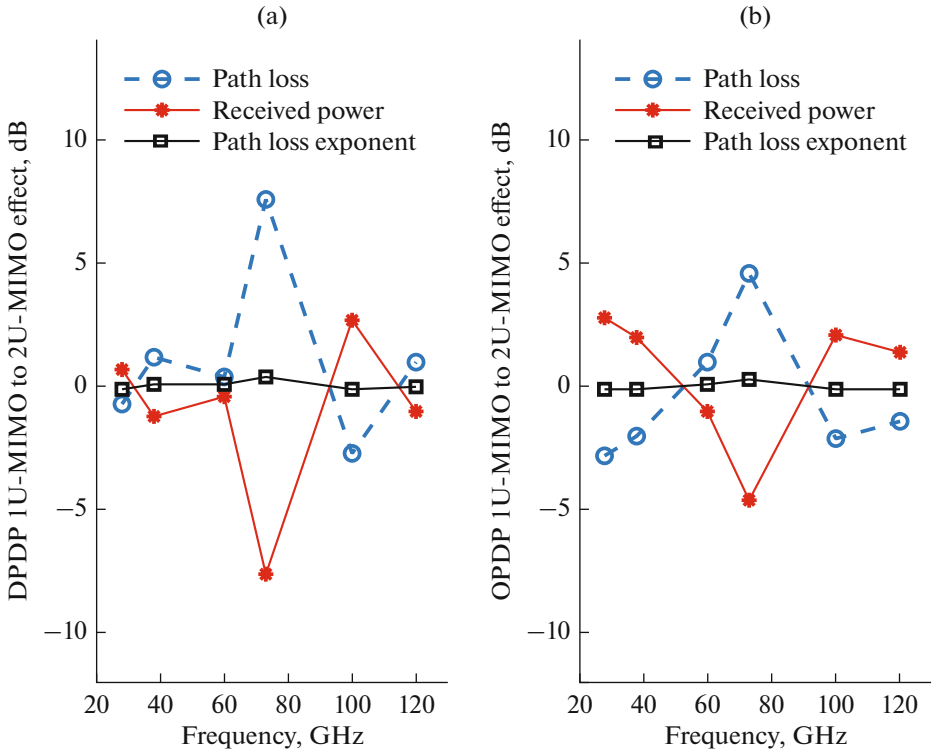

Fig. 29. Effect of changing from 1U-MIMO to 2U-MIMO channel for: (a) DPDP, (b) OPDP.

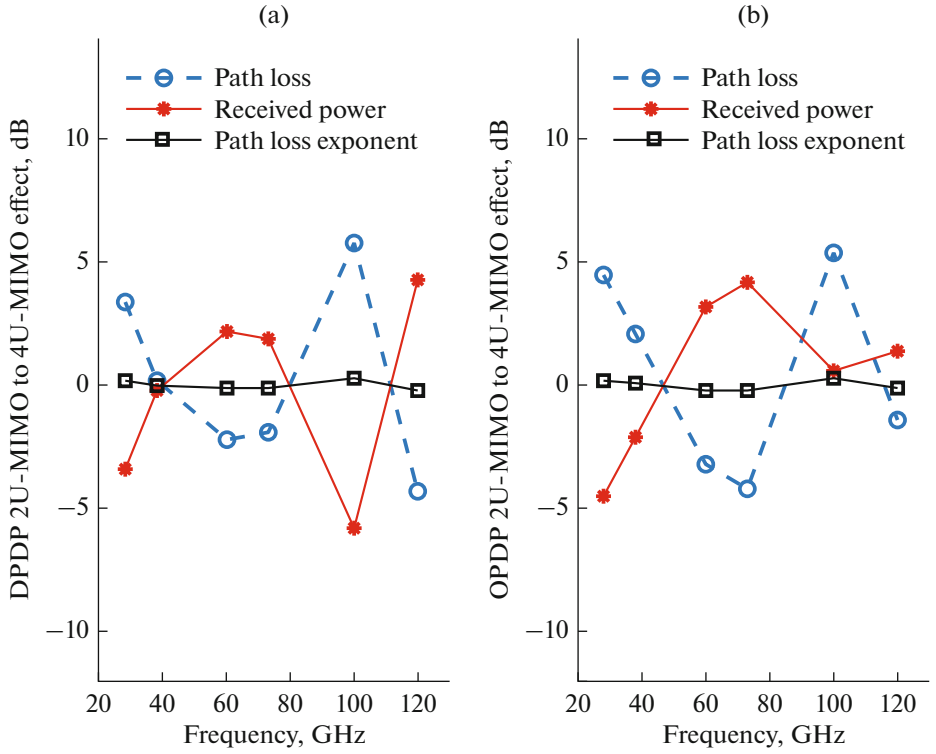

Fig. 30. Effect of changing from 2U-MIMO to 4U-MIMO channel for: (a) DPDP, (b) OPDP.

PL and received power (2 dB), while the 38 GHz channel is less affected compared to the other channels (0.2 dB). All channels have approximately the same effect on the PLE.

4. CONCLUSIONS

Summing up the results, it can be concluded that the parameters of statistical channel modeling are dependent on the geometric parameters (Co-Pol/X-Pol, SISO/SIMO/MIMO) and environmental conditions (LOS/NLOS, rain rate, temperature and humidity). Furthermore, the MU–MIMO scenario affect is investigated, mainly the impact of switching from 1U-MIMO to 2U-MIMO or 2U-MIMO to 4U-MIMO, this scenario is not taken into account in recent works. The study of this work aims to illustrate mmWave characteristics (PL, PLE, Received power) at 28, 38, 60, 73, 100, and 120 GHz. Overall observation suggests that mmWave channel with carrier frequencies 28, 60, 100, and 120 GHz channels are more affected by the switching from LOS to NLOS. However, 38 GHz channel is the least affected, nevertheless, channel 73 GHz is more tolerant of the LOS to NLOS effect. Besides, in terms of antenna configurations (SISO/SIMO/MIMO), the results indicated that 120 GHz is more affected, while 28 GHz is less affected than the other channels, except that 38 GHz is more favorable to change this factor. For rain, temperature and humidity factors, it was concluded that the attenuations of 60, 100 and 120 GHz are the most important, while 28 and 73 GHz channels are less affected, except that 38 channel is the most capable to withstand the change of these factors. After comparing our results with those from the literature, we have concluded that rain fade depends to link length. Finally, the OPDP exhibits a lower attenuation index and attenuation exponent than the DPDP. This proposed work will be highly useful for 5G/6G research and system deployment and expected to help future engineers to design an efficient mmWave channel modeling for new outdoor scenarios. As a future perspective, the spatial study can be beneficial in showing and planning the measurable channel models for future 5G/6G millimeter wave communications.

FUNDING

This work was supported by Directorate General for Scientific Research and Technological Development (DGRSDT), Ministry of Higher Education and Scientific Research – Algeria.

CONFLICT OF INTEREST

The authors declare that they have no conflicts of interest.

REFERENCES

1. W. Saad, M. Bennis, and M. Chen, "A Vision of 6G wireless systems: Applications, trends, technologies, and open research problems," IEEE Network, **34** (3), 134–142 (2020). https://doi.org/10.1109/MNET.001.1900287
2. M. Z. Chowdhury, M. Shahjalal, S. Ahmed, and Y. M. Jang, "6G wireless communication systems: Applications, requirements, technologies, challenges, and research directions," IEEE Open J. Commun. Soc. **1**, 957–975 (2020). https://doi.org/10.1109/OJCOMS.2020.3010270
3. T. S. Rappaport, Y. Xing, G. R. MacCartney, A. F. Molisch, E. Mellios, and J. Zhang, "Overview of millimeter wave communications for fifth-generation (5G) wireless networks—With a focus on propagation models," IEEE Trans. Antennas Propag. **65**, 6213–6230 (2017). https://doi.org/10.1109/TAP.2017.2734243
4. M. Giordani, M. Polese, M. Mezzavilla, S. Rangan, and M. Zorzi, "Toward 6g networks: Use cases and technologies," IEEE Commun. Mag. **58**, 55–61 (2020). https://doi.org/10.1109/MCOM.001.1900411
5. W. Ali, S. Das, H. Medkour, and S. Lakrit, "Planar dual-band 27/39 GHz millimeter-wave MIMO antenna for 5G applications," Microsys. Technol. **27** (1), 283–292 (2021). https://doi.org/10.1007/s00542-020-04951-1
6. U. R. Kamboh, U. Ullah, S. Khalid, et al., "Path loss modelling at 60 GHz mmWave based on cognitive 3D ray tracing algorithm in 5G," Peer-to-Peer Netw. Appl. **14**, 3181–3197 (2021). https://doi.org/10.1007/s12083-021-01101-w
7. M. S. Sim, Y. G. Lim, S. H. Park, L. Dai, and C. B. Chae, "Deep learning-based mmWave beam selection for 5G NR/6G with sub-6 GHz channel information: Algorithms and prototype validation," IEEE Access, **8**, 51634–51646 (2020). https://doi.org/10.1109/ACCESS.2020.2980285
8. H. Ullah and F. A. Tahir, "A high gain and wideband narrow-beam antenna for 5G millimeter-wave applications," IEEE Access. **8**, 29430–29434 (2020). https://doi.org/10.1109/ACCESS.2020.2970753
9. Begishev et al., "Performance analysis of multi-band microwave and millimeter-wave operation in 5G NR systems," in IEEE Trans. Wireless Commun. **20** (6), 3475–3490 (2021). https://doi.org/10.1109/TWC.2021.3051027
10. Rony Kumer Saha,"Spectrum allocation and reuse in 5G new radio on licensed and unlicensed millimeter-wave bands in indoor environments," Mobile Inf. Syst. **2021** ArticleID 5538820, (2021). https://doi.org/10.1155/2021/5538820
11. FC Commission, "FCC takes steps to open spectrum horizons for new services and technologies," [Online]. Available: https://docs.fcc.gov/public/attachments/DOC-356588A1.pdf.
12. S. Ju, Y. Xing, O. Kanhere, and T. S. Rappaport, "Millimeter wave and sub-terahertz spatial statistical channel model for an indoor office building," IEEE J. Se-

lected Areas in Commun. **39**, 1561–1575 (2021). https://doi.org/10.1109/JSAC.2021.3071844

13. R. H. Clarke, "A statistical theory of mobile-radio reception," Bell System Tech. J. **47**, 957–1000 (1968). https://doi.org/10.1002/j.1538-7305.1968.tb00069.x
14. J. I. Smith,"A computer generated multipath fading simulation for mobile radio," IEEE Trans. Vehicular Technol. **24**, 39–40 (1975). https://doi.org/10.1109/T-VT.1975.23600
15. T. S. Rappaport, S. Y. Seidel, and K. Takamizawa,"Statistical channel impulse response models for factory and open plan building radio communicate system design," IEEE Trans. Commun. **39**, 794–807 (1991). https://doi.org/10.1109/26.87142
16. V. Fung, T. S. Rappaport, and B. Thoma, "Bit error simulation for pi /4 DQPSK mobile radio communications using two-ray and measurement-based impulse response models," in IEEE J. Selected Areas in Commun. **11**, 393–405 (1993). https://doi.org/10.1109/49.219546
17. C. Cheng, S. Kim, and A. Zajić, "Comparison of path loss models for indoor 30 GHz, 140 GHz, and 300 GHz channels," in *Proc. 11th Eur. Conf. on Antennas and Propagation (EUCAP) 2017* (EuCAP, 2017), pp. 716–720. https://doi.org/10.23919/EuCAP.2017.7928124
18. S. Sun, T. S. Rappaport, M. Shafi, P. Tang, J. Zhang, and P. J. Smith, "Propagation models and performance evaluation for 5G millimeter-wave bands," in IEEE Trans. Vehicular Technol. **67**, 8422–8439 (2018). https://doi.org/10.1109/TVT.2018.2848208
19. S. Agrawal and K. Sharma, "5th generation millimeter wave wireless communication propagation losses dataset for indian metro cities based on corresponding weather conditions," Data in brief, **23**,103564 (2019). https://doi.org/10.1016/j.dib.2018.12.003
20. S. Ju, O. Kanhere, Y. Xing, and T. S. Rappaport," A millimeter-wave channel simulator NYUSIM with spatial consistency and human blockage," in *Proc. IEEE Global Communications Conf. (GLOBECOM),Waikoloa, HI, USA, Dec. 9–13, 2019*, (GLOBECOM, 2019), pp. 1–6. https://doi.org/10.1109/GLOBECOM38437.2019.9013273
21. T. S. Rappaport et al.,"Millimeter wave mobile communications for 5G cellular: It Will Work!," IEEE Access **1**, 335–349 (2013). https://doi.org/10.1109/ACCESS.2013.2260813
22. S. Sun, G. R. MacCartney, and T. S. Rappaport, "A novel millimeter-wave channel simulator and applications for 5G wireless communications," in *Proc. IEEE Int. Conf. on Commun. (ICC), 2017* (ICC, 2017), pp. 1–7. https://doi.org/10.1109/ICC.2017.7996792
23. 3GPP Radio Access Network Working Group, "Study on channel model for frequencies from 0.5 to 100 GHz (Release 15)," 15, 3GPP TR 38.901 (2018).
24. P. Kyosti, "WINNER II channel models," IST, Tech. Rep. IST-4-027756 WINNER II D1. 1.2 V1. 2 (2007).
25. A. A. Budalal, M. R. Islam, M. H. Habaebi, and T. A. Rahman," Millimeter Wave Channel Modeling – Present Development and Challenges in Tropical Areas," in *Proc. 7th Int. Conf. Computer and Commun. Engineering (ICCCE), Hyderabad, India, 2018*, pp. 23–28 (2018). https://doi.org/10.1109/ICCCE.2018.8539324
26. R. Hasan, M. M. Mowla, M. A. Rashid, M. K. Hosain, and I. Ahmad, "A Statistical Analysis of Channel Modeling for 5G mmWaves Communications," in *Int. Conf. on Electrical, Computer and Commun. Engineering (ECCE), Baltimore, Maryland, Sept. 29–Oct. 3, 2019*, pp. 1–6 (2019). https://doi.org/10.1109/ECACE.2019.8679507
27. C. Han, Y. Bi, S. Duan, and G. Lu, "Rain rate retrieval test from 25-GHz, 28-GHz, and 38-GHz millimeter-wave link measurement in Beijing," IEEE J. of Selected Topics in Applied Earth Observations and Remote Sensing, **12**, 2835–2847 (2019). https://doi.org/10.1109/JSTARS.2019.2918507
28. D. Nandi and A. Maitra, "The effects of rain on millimeter wave communication for tropical region," in *URSI Asia-Pacific Radio Sci. Conf. (AP-RASC), New Delhi, India, Mar. 10–14, 2019* (AP-RASC, 2019), pp. 1–3. https://doi.org/10.23919/URSIAP-RASC.2019.8738591
29. H. B. Hamid Dutty and M. M. Mowla, "Weather impact analysis of mm waves channel modeling for aviation backhaul networks in 5G communications,"in *22nd Int. Conf. on Computer and Information Technology (ICCIT), Tejgaon, Dhaka, Bangladesh, 2019*, (ICCIT, 2019), pp. 1–6. https://doi.org/10.1109/ICCIT48885.2019.9038447
30. R. Rudd, K. Craig, M. Ganley, and R. Hartless, "Building Materials and Propagation," Final Report; Ofcom: London, UK, 2604 (2014).
31. T. S. Rappaport, G. R. MacCartney, M. K. Samimi, and S. Sun, "Wideband millimeter-wave propagation measurements and channel models for future wireless communication system design," IEEE Trans. on Commun. **63**, 3029–3056 (2015). https://doi.org/10.1109/TCOMM.2015.2434384
32. Y. Xing, O. Kanhere, S. Ju, T. S. Rappaport, and G. R. MacCartney, "Verification and calibration of antenna cross-polarization discrimination and penetration loss for millimeter wave communications,"in *Proc. IEEE 88th Vehicular Technol. Conf. (VTC–Fall), Chicago, IL, USA, Aug. 27–30, 2018* (IEEE, New York, 2018), pp. 1–6 (2018). https://doi.org/10.1109/VTCFall.2018.8690683
33. M. K. Samimi and T. S. Rappaport, "3-D millimeter-wave statistical channel model for 5G wireless system design," IEEE Trans. on Microwave Theory and Techniques, **64**, 2207–2225 (2016). https://doi.org/10.1109/TMTT.2016.2574851
34. T. S. Rappaport, S. Sun, and M. Shafi, "Investigation and comparison of 3GPP and NYUSIM channel models for 5G wireless communications," in *IEEE 86th Vehicular Technology Conf. (VTC-Fall), Toronto, ON, Canada, Sept. 24–27, 2017* (IEEE, New York, 2017), pp. 1–5. https://doi.org/10.1109/TVT.2018.2848208
35. M. S. Kumari and N. Kumar, "Channel model for simultaneous backhaul and access for mmWave 5G outdoor street canyon channel," Wireless Networks, **26**, 5997–6013 (2020). https://doi.org/10.1007/s11276-020-02421-0

36. Momo, Sumaiya Haq Aftabi, and Md Munjure Mowla, "Statistical analysis of an outdoor mmWave channel model at 73 GHz for 5G networks," in *Proc. IEEE Int. Conf. on Computer, Communication, Chemical, Materials and Electronic Engineering (IC4ME2), 2019* (IEEE, New York, 2019), pp. 1–4 (2019). https://doi.org/10.1109/IC4ME247184.2019.9036692

37. Shamsan, Zaid Ahmed, "Astatistical channel propagation analysis for 5G mm wave at 73 GHz in Urban Microcell, " in *Int. Conf. Reliable Information and Communication Technology, Springer, Cham, 2020* (Springer-Verlag, 2020), pp. 748–756 (2020). https://doi.org/10.1007/978-3-030-70713-2_68

38. H. B. H. Dutty, M. M. Mowla, and M. A. Mou, "Millimeter wave channel modeling for aviation backhaul networks in 5g communications," in *Proc. 22nd Int. Conf. on Computer and Inf. Technol. (ICCIT), Tejgaon, Dhaka, Bangladesh, 2019*, (ICCIT, 2019), pp. 1–5. https://doi.org/10.1109/ICCIT48885.2019.9038586

39. R. Hasan, M. M. Mowla, and M. Khatun, "The impact of linear polarization on channel modeling in 5G cellular communications: A Statistical approach," in *Proc. IEEE 5th Int. Conf. on Advances in Electrical Engineering* (ICAEE), Sept. 26–28, Dhaka, Bangladesh, 2019 (IEEE, New York, 2019), pp. 329–334 (2019). https://doi.org/10.1109/ICAEE48663.2019.8975579

40. T. S. Rappaport, Y. Xing, O. Kanhere, S. Ju, A. Madanayake, S. Mandal, and G. C. Trichopoulos, "Wireless communications and applications above 100 GHz: Opportunities and challenges for 6G and beyond," IEEE Access **7**, 78729–78757 (2019). https://doi.org/10.1109/ACCESS.2019.2921522

41. M. I. Kamrul, K. Mazharul Haque, and M. M. Amir Faisal, "Performance evaluation of MIMO in Urban Microcell for Dhaka City at 28 GHz frequency," in *Proc. IEEE Int. Conf. on Innovations in Science, Engineering and Technology, (ICISET) 2018*, (ICISET, 2018,) pp. 427–431. https://doi.org/10.1109/ICISET.2018.8745660

42. A. A. Budalal, I. M. Rafiqul, M. H. Habaebi, and T. A. Rahman, "The effects of rain fade on millimetre wave channel in tropical climate," Bull. Electr. Eng. and Inf. **8**, 653–664 (2019). https://doi.org/10.11591/eei.v8i2.1487

43. A. Al-Shuwaili and T. M. Jamel, "5G channel characterization at millimeter-wave for baghdad city: An NYUSIM-based approach," in *Proc. IEEE 18th Int. Multi-Conf. on Systems, Signals & Devices (SSD), Monastir, Tunisia, March, 22–25, 2021* (IEEE, New York, 2021), pp. 468–473. https://doi.org/10.1109/SSD52085.2021.9429348